

**ENERGY AND EXERGY DIAGNOSTICS OF AN INDUSTRIAL ANNULAR SHAFT
LIMEKILN WORKING WITH PRODUCER GAS AS RENEWABLE BIOFUEL**

Tomás Pessoa Londe Camargos¹, Andréa Oliveira Souza da Costa^{1,2,*}, Esly Ferreira Costa Junior^{1,2}

¹ Graduate Program in Mechanical Engineering, Federal University of Minas Gerais, Belo Horizonte – Minas Gerais, Brazil

² Graduate Program in Chemical Engineering, Federal University of Minas Gerais, Belo Horizonte – Minas Gerais, Brazil

<https://doi.org/10.2298/CICEQ231020011C>

Received 20.10.2023.

Revised 21.2.2024.

Accepted 29.3.2024.

* Andréa Oliveira Souza da Costa (corresponding author), **Address:** Department of Chemical Engineering, Av. Pres. Antônio Carlos, 6627 - Pampulha, Belo Horizonte - MG, Brazil, 31270-901. **E-mail:** andreacosta@deq.ufmg.br, **Phone:** +55 31 3409 3601.

ABSTRACT

Quicklime, a globally significant commodity used in various industrial applications, is produced in limekilns requiring substantial energy, traditionally, from fossil fuels. However, due to escalating emission constraints and depletion of fossil fuel deposits, the quicklime industry explores alternative fuels, like biomass. The literature lacks feasibility diagnostic studies on limekilns using alternative biomass fuels. Thus, this article aims to conduct energy and exergy diagnostics on an industrial limekiln using producer gas derived from eucalyptus wood as renewable biofuel. Employing industrial data and thermodynamics principles, the equipment was characterized, and results were compared with literature findings for similar limekilns using fossil fuels. The Specific Energy Consumption (SEN) for the producer gas-operated limekiln was $4.8 \text{ GJ/t}_{\text{quicklime}}$, with energy (η_{en}) and exergy (η_{ex}) efficiencies of 54.6% and 42.2%. Overall energy ($\eta_{en-overall}$) and exergy ($\eta_{ex-overall}$) efficiencies were 42.0% and 23.6%, respectively, lower than literature values. $SEN_{overall}$ was $7.6 \text{ GJ/t}_{\text{quicklime}}$, higher than literature results. Identified enhancements for both renewable and fossil fuel-powered limekilns involve recovering energy and exergy, including heat recovery from exhaust gases, minimizing thermal losses, and optimizing operational variables. These findings offer valuable insights for researchers exploring renewable biofuel adoption, like producer gas derived from eucalyptus wood, as alternatives to conventional fossil fuels in limekilns.

KEYWORDS: energy, exergy, limekiln, quicklime, biomass, biofuel.

Highlights

- Performance results for a limekiln operating with renewable biofuel were presented;
- The new results exposed come from energy and exergy diagnostics of the limekiln;
- Energy and exergy efficiencies of the limekiln were 54.6 and 42.2%, respectively;
- Energy and exergy global efficiencies of calcination process were 42.0 and 23.6%, respectively;
- Results showed that producer gas as renewable biofuel can be competitive.

INTRODUCTION

Quicklime is a solid substance with $\text{CaO}_{(s)}$ as its main constituent, and it holds global significance due to its various essential applications as a chemical compound. These applications include its use in mortar and cement production, water treatment, air pollution control, glass manufacturing, whitewashing acidic soils, casting steps, and as a chemical absorbent [1]. Moreover, the literature has explored innovative applications and properties of quicklime, such as its use for: adsorbent development [2], novel composite material development [3] and water transfer mechanism of quicklime modified centrifugal dewatering clay [4].

Among the top five global quicklime producers in 2019 are China, India, USA, Russia, and Brazil. Brazil ranks fifth in this list and produced approximately 8.1 million metric tons of quicklime in 2019 [5].

Limestone, predominantly composed of $\text{CaCO}_{3(s)}$, is utilized as the raw material for the manufacture of quicklime. In this process, either horizontal or vertical limekilns are employed, where temperatures around 900 – 1000 °C are reached by the limestone, leading to the thermal decomposition of $\text{CaCO}_{3(s)}$ into $\text{CaO}_{(s)}$ and $\text{CO}_{2(g)}$. The heat necessary for the calcination reaction in limekilns is traditionally generated through the combustion of fossil fuels [6].

The most significant factor influencing quicklime production cost is fuel consumption, which accounts for approximately 50% of the total manufacturing cost [7]. In addition to cost considerations, quicklime production stands out as one of the industrial processes with the highest emissions of $\text{CO}_{2(g)}$ [8]. Specifically during limestone calcination, 785 kg of $\text{CO}_{2(g)}$ are emitted per ton of $\text{CaCO}_{3(s)}$, and an additional 200 – 400 kg of $\text{CO}_{2(g)}$ are emitted during fuel combustion. This results in a total emission of around 1000 – 1200 kg of $\text{CO}_{2(g)}$ per ton of produced quicklime [7]. As the $\text{CO}_{2(g)}$ produced during $\text{CaCO}_{3(s)}$ calcination remains constant, the total emitted $\text{CO}_{2(g)}$ depends primarily on the fuel consumption efficiency within the limekiln [7].

For these reasons aforementioned, studies aiming to improve the calcination process have been undertaken by authors from various countries across the globe, such as: Australia [9], China [10, 11], Germany [12], India [13] and Indonesia [14]. However, for Brazil, the fifth largest quicklime producer in the world, there is a gap in the literature regarding studies involving energy and exergy analyses of limekilns operating with renewable biofuels.

The energy efficiency of limekilns can be defined as the ratio between the thermal energy required for the calcination reaction and the energy released by the fuel. Vertical limekilns exhibit higher efficiency (approximately 65–77%) compared to rotary ones (about 40–52%) [15]. Moreover, the Vertical Regenerative Parallel Flow type shows the highest efficiency (around 80–90%), despite its

recent technological maturity [6]. These energy analyses have inherent limitations since they consider solely the first law of thermodynamics [16].

Therefore, exergy analyses can overcome these limitations by incorporating both the first and second laws of thermodynamics. Thus, exergy analyses contribute significantly to the diagnostics of thermodynamic processes, providing a broader understanding of a process and its sustainability, being able to identify specific parameters to improve the equipment performance, such as: irreversibilities points, exergy losses and fuel saving points [16].

There are studies in the literature in which energy and exergy analyses of limekilns operating with traditional fossil fuels were performed [7, 16]. However, works addressing energy and exergy analyses of limekilns operating with renewable biofuels, such as the present study, were not found in the literature. The current authors have recently conducted experimental analyses involving energy and exergy assessments of other types of equipment, including compressed air energy storage systems [17], kraft biomass boilers [18], clinker rotary kilns [19], and specific chemical exergy predictions for biological molecules [20].

In thermal energy production, the burning of fossil fuels corresponds to one of the main sources of greenhouse gas emissions, mainly $\text{CO}_{2(g)}$, which can lead to climate changes. Additionally, the depletion of fossil fuel deposits can also imply limitations in the future regarding their uses as energy sources [21]. However, in this scenario, the limekilns are heavily dependent on the employment of solid fossil fuels, oil and natural gas to meet the equipment's energy demand. These three fossil fuels together represent an employment share of around 90% of the types of fuels used in limekilns [22]. Of these fossil fuels, natural gas is the option that results in the lowest greenhouse gas emissions. Nevertheless, natural gas has a high cost compared to other fossil fuels employed in limekilns.

For these reasons, the lime sector has sought to use other fuel types that meet the increasing limitations on atmospheric emissions, greenhouse gases, product quality and reduction of quicklime production costs. Favorably, with the deployment of renewable biomass fuels, these requirements aforementioned can be satisfactorily met, which makes biomass an attractive solution for use as biofuel in limekilns. Despite this, the utilization of biomass still represents a small portion of around 2% of the fuels utilized in limekilns [22].

Given the preceding points, it can be perceived that there is a lack of literature regarding energy and exergy diagnostic studies of limekilns operating with biofuels. It is in this regard that the current work aims to contribute to the scientific community. Hence, the aim of the current paper is to conduct energy and exergy diagnostics of a vertical annular shaft limekiln operating with producer gas as a renewable biofuel. To attain this objective, technical visits were made to a calcination industry in

the state of Minas Gerais, Brazil. In this company, it was investigated *in situ* how its calcination process is realized, and the employment of producer gas was verified as a renewable biofuel derived from the gasification of eucalyptus wood used as raw material. Operational data of the calcination process were collected at the aforementioned industry. The applied methodology employed to undertake the diagnostics of the annular shaft limekiln was based on the first and second laws of thermodynamics and on mass, energy, and exergy balances of the equipment. Thus, through the proposed diagnostics, investigations were conducted to assess the energy and exergy efficiencies of the limekiln and of the calcination process overall, identify points of exergy loss, analyze potential points for exergy recovery, evaluate destroyed exergy, and examine the energy and exergy content of the equipment flows. The results obtained in this study for the limekiln performing with renewable biofuel were compared with literature results for similar vertical annular shaft limekilns operating with traditional fossil fuels. The Specific Energy Consumption (SEN) obtained from the limekiln operating with producer gas was 4.8 GJ per ton of quicklime produced, with energy (η_{en}) and exergy (η_{ex}) efficiencies of 54.6% and 42.2%, respectively. The overall energy ($\eta_{en-overall}$) and exergy ($\eta_{ex-overall}$) efficiencies of the calcination process were 42.0% and 23.6%, respectively. The $SEN_{overall}$ of the calcination process was 7.6 GJ per ton of quicklime produced. It was verified that the usage of producer gas as a biofuel derived from eucalyptus wood is technically feasible, sustainable, and can be a solution to the conventional fossil fuels employed in limekilns. Noteworthy enhancements for both renewable and fossil fuel-powered limekilns encompass the recuperation of energy and exergy. This includes mainly heat recovery from exhaust gases, reduction of thermal losses, and optimization of operational parameters. The performance of the calcination process can be improved through the aforementioned suggestions, leading to potential fuel savings and the subsequent reduction in costs and pollutant gas emissions. In addition to the aforementioned contributions, it is expected that this work can also reduce the lack of energy and exergy diagnostics for limekilns operating in Brazil, the fifth-largest global quicklime producer.

MATERIALS AND METHODS

In this section, the approach utilized for conducting the present study is presented, concerning the characterization of the calcination process, identification of its temperature measurement points, formulation of assumed hypotheses, descriptions of the collected data, and properties of the constituent species of the system.

Limekiln characterization

Technical visits were conducted to a calcination company in Minas Gerais, Brazil, where an on-site examination of a vertical annular shaft limekiln was carried out for its operational characterization.

Figure 1 depicts the aforementioned annular shaft limekiln, with the Control Volume (CV) encompassing the equipment in continuous operation. It was considered that the equipment operates in steady state, with constant inlet and outlet conditions, and without mass accumulation. This assumption is proper and commonly considered by the literature for limekilns similar to the one investigated herein [6, 16]. The vertical annular shaft limekiln has a cylindrical shape, height of 22 m, diameter of 3.2 m, and wall thickness of 0.4 m. The inner wall of the limekiln is coated with refractory material.

As shown in Figure 1, eight mass flows i (m_i) cross the Control Volume (CV), where i represents the substance contained in the flow and is denoted in the subscript as ls , lm , $ls - ub$, pg , a , pc , $CO_{2(g)} - cr$ e sw , representing limestone, quicklime, unburned limestone, producer gas, combustion air, combustion products, $CO_{2(g)}$ released in limestone calcination, and solid waste, respectively. This same nomenclature was also used throughout the current paper to describe a substance contained in a certain flow.

Therefore, as depicted in Figure 1, a mass flow of limestone (m_{ls}) is introduced at the top of the limekiln, while a mass flow of produced quicklime (m_{lm}) exits simultaneously from the bottom. Due to gravity, limestone (m_{ls}) moves downward and when it reaches the decarbonation temperature in the Calcination Zone it reacts forming $CaO_{(s)}$ and $CO_{2(g)}$. At the bottom of the limekiln, a mass flow of unburnt limestone (m_{ls-ub}) exits, which consists of limestone that does not undergo calcination. A mass flow of producer gas (m_{pg}), the renewable biofuel, is introduced into the Calcining Zone along with a mass flow of combustion air (m_a). In the Calcination Zone, the producer gas distribution system is assembled to feed the biofuel (m_{pg}) through burners, providing the heat of combustion axially and radially in the combustion chamber. In this same region, the combustion air (m_a) is introduced with the assistance of air blowers. In the Cooling Zone, in practice, air is also introduced, which comes into contact with the quicklime in this region, cooling it. As a result, this heated air flows upward in countercurrent with the quicklime bed. This ascending heated air not only aids in biofuel combustion but also preheats the limestone at the top of the limekiln. The cooling air was assumed to be a portion of the combustion air (m_a). From the Preheating Zone, with the aid of an exhauster, in a single flow are released: the mass flow of combustion products (m_{pc}) arising from the burn of the producer gas; the mass flow of $CO_{2(g)}$ ($m_{CO_{2(g)}-cr}$) produced from the limestone calcination; and the mass flow of solid waste (m_{sw}) resulting from limestone attrition.

For operational control of the limekiln, the monitoring of three temperatures is performed at specific points as indicated in Figure 1: Temperature A (T_A) is measured at the supply of producer gas; Temperature B (T_B) is measured at the limekiln top; and Temperature C (T_C) is controlled at the outlet of the quicklime and unburnt limestone flows at the bottom of the equipment.

Figure 1

Data collection

Table 1 presents the collected data provided by the company regarding its calcination process during regular working periods, concerning the quantities of component flows, operational temperatures, and chemical composition of limestone and quicklime. Literature data for the chemical composition of producer gas and eucalyptus wood are also provided to complement the system characterization. Additionally, the data for the specific heat polynomials used in the energy and exergy diagnostics are included.

Table 1

To convert masses of chemical species (m) to their corresponding moles (n), the tabulated molar masses (MM) provided by [23] were utilized.

Temperature characterization

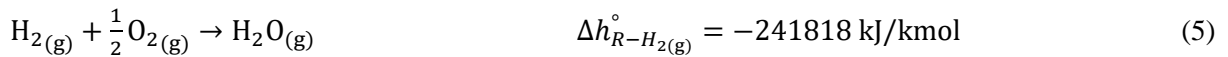
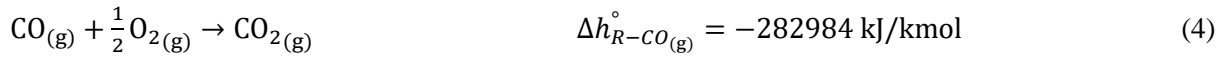
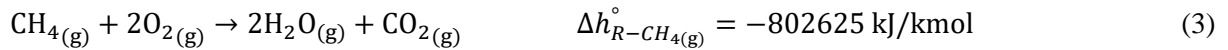
The temperatures (T_i) of the mass flows i (m_i) that cross the limekiln's CV described in Figure 1 are stated in this subsection. For the mass flow of producer gas (m_{pg}) it was considered that its temperature (T_{pg}) corresponds to $T_A = 387.2$ °C. Regarding the mass flows of products of combustion (m_{pc}), $CO_{2(g)}$ from calcination ($m_{CO_{2(g)}-cr}$) and solid wastes (m_{sw}) the temperatures T_{pc} , $T_{CO_{2(g)}-cr}$ and T_{sw} were respectively considered, at $T_B = 198.2$ °C. For the mass flows of quicklime (m_{lm}) and unburnt limestone (m_{ls-ub}), the temperatures T_{lm} and T_{ls-ub} were respectively considered, as being $T_C = 60.0$ °C. For the mass flows of limestone (m_{ls}) and combustion air (m_a) the temperatures T_{ls} and T_a were respectively defined, as being at ambient temperature $T_{env} = 25.0$ °C.

Characterization of standard heats of reaction

The chemical species $\text{CaCO}_{3(s)}$ and $\text{CaCO}_3 \cdot \text{MgCO}_{3(s)}$ that constitute the limestone entering the limekiln undergo calcination according to Equations 1 and 2, respectively. The standard heats of reaction at 298 K of $\text{CaCO}_{3(s)}$ ($\Delta h_{R-\text{CaCO}_{3(s)}}^\circ$) and $\text{CaCO}_3 \cdot \text{MgCO}_{3(s)}$ ($\Delta h_{R-\text{CaCO}_3 \cdot \text{MgCO}_{3(s)}}^\circ$) were characterized using standard heats of formation (Δh_{298}°) tabulated and reported by literature [24–27]. The chemical species $\text{SiO}_{2(s)}$, $\text{Al}_2\text{O}_{3(s)}$ and $\text{Fe}_2\text{O}_{3(s)}$ that constitute the limestone are inert.



For the producer gas, its constituent chemical species $\text{CH}_{4(g)}$, $\text{CO}_{(g)}$ and $\text{H}_{2(g)}$ undergo combustion according to the chemical reactions expressed by Equations 3, 4 and 5, respectively. The heats of combustion reaction of $\text{CH}_{4(g)}$ ($\Delta h_{R-\text{CH}_{4(g)}}^\circ$), $\text{CO}_{(g)}$ ($\Delta h_{R-\text{CO}_{(g)}}^\circ$) and $\text{H}_{2(g)}$ ($\Delta h_{R-\text{H}_{2(g)}}^\circ$) were also characterized employing the Δh_{298}° tabulated and provided by literature [24–27]. The other chemical species that constitute the producer gas, which are $\text{CO}_{2(g)}$, and $\text{N}_{2(g)}$, do not undergo combustion.



Characterization of chemical species constituting the mass flows

Each mass flow i (m_i) that crosses the limekiln's CV, is a mixture of solid or gases constituted by chemical species j . The species j constituting the mass flows of limestone (m_{ls}), quicklime (m_{lm}) and producer gas (m_{pg}) were mentioned in their chemical compositions presented in Table 1. The mass flow of combustion air is composed of molar proportion of 21% $\text{O}_{2(g)}$ and 79% $\text{N}_{2(g)}$, since the air inserted is atmospheric. The species j that constitute m_{ls} , also compose the mass flows of unburnt limestone (m_{ls-ub}) and solid waste (m_{sw}) arising from limestone friction. The mass flow of combustion products consists of $\text{CO}_{2(g)}$, $\text{O}_{2(g)}$, $\text{N}_{2(g)}$ and $\text{H}_2\text{O}_{(g)}$, according to the reactions described in Equations 3, 4 and 5 and considering air excess commonly employed in limekilns.

Specific heat

For the specific heats (Cp_j) of chemical species j constituents of the mass flows (m_i) that cross the limekiln's CV, the characteristic polynomials as a temperature function, characterized by Equations 6 to 8, were considered according to the references indicated. The coefficients of these equations for each chemical species are presented in Table 1, as well as their temperature validity ranges and corresponding equations. The mass flow temperatures i (T_i) must be utilized in Kelvin. In Equations 7 and 8, the Cp_j output unit is kJ/(kmol·K). In Equation 6, the Cp_j/R ratio is used by the reference to make the equation dimensionless, and the Cp_j output unit is the same of the universal gas constant (R) employed in this work, which was 8.31446 kJ/(kmol.K).

$$Cp_j/R = A + B \cdot T_i + C \cdot T_i^2 + D \cdot T_i^{-2} \quad (6) [24]$$

$$Cp_j = A + B \cdot T_i - C \cdot T_i^{-2} \text{ kJ}/(\text{kmol} \cdot \text{K}) \quad (7) [25]$$

$$Cp_j = A + B \cdot t_i + C \cdot t_i^2 + D \cdot t_i^3 + E \cdot t_i^{-2} \text{ kJ}/(\text{kmol} \cdot \text{K}) \quad t_i = T_i/1000 \quad (8) [26]$$

MATHEMATICAL DESCRIPTION

The data, characterizations and considerations previously provided were utilized in the mathematical description described separately in the following. Although the procedure employed is for a vertical annular shaft limekiln operating with producer gas as a renewable biofuel, in general it can be replicated to other types of renewable biofuels and limekilns.

Mass Balance

The limekiln's CV was schematically illustrated in Figure 2(a) with the mass flows i (m_i) involved. Limekilns are commonly and properly analyzed in the literature as operating in steady state, as the equipment works continuously with constant inlet and outlet conditions [6, 16]. So, in Equation 9, applying the mass conservation principle and considering steady state, it is implied that the sum of input mass flows i (m_{in-CV}) is equivalent to the sum of output mass flows i (m_{out-CV}) in kg/h:

Figure 2

$$\sum m_{in-CV} = \sum m_{out-CV} \quad (9)$$

no mass is accumulated in CV, therefore, substituting in Equation 9 the mass flows (m_i) of CV, it results in:

$$m_{ls} + m_{pg} + m_a = m_{lm} + m_{eg} + m_{ls-ub} + m_{sw} \quad (10)$$

where the mass flows correspond to: limestone (m_{ls}), producer gas (m_{pg}), combustion air (m_a), quicklime (m_{lm}), exhaust gases (m_{eg}), unburnt limestone (m_{ls-ub}) and solid waste (m_{sw}).

The mass flow of exhaust gases (m_{eg}) is characterized by the sum of the mass flows of combustion products (m_{pc}) and CO_{2(g)} generated in calcination ($m_{CO_2(g)-cr}$), thus:

$$m_{eg} = m_{pc} + m_{CO_2(g)-cr} \quad (11)$$

Each mass flow i (m_i) in Equation 10 is a mixture of solid or gases composed by the sum of the masses of constituent chemical species j (m_j) characterized in the previous chapter, as follows:

$$m_i = \sum_{j=1}^p m_j \quad (12)$$

The evaluation of the combustion air quantity for the producer gas was performed using stoichiometry and considering an excess of air. Thus, initially, based on the combustion reactions of the producer gas characterized by Equations 3 to 5, the stoichiometric number of moles of oxygen ($n_{O_2(g)-ST}$) was determined as:

$$n_{O_2(g)-ST} = \left(n_{CH_4(g)-pg} \cdot 2 + \frac{n_{CO(g)-pg}}{2} + \frac{n_{H_2(g)-pg}}{2} \right) \quad (13)$$

in which $n_{CH_4(g)-pg}$, $n_{CO(g)-pg}$ and $n_{H_2(g)-pg}$ are the mole numbers of the species indicated in the subscripts present in the producer gas, whose percentages for each component were provided in Table 1 and can be expressed in terms of the mole number of the producer gas (n_{pg}) as follows:

$$n_{CH_4(g)-pg} = 0.07 \cdot n_{pg} \quad (14)$$

$$n_{CO_{(g)}-pg} = 0.14 \cdot n_{pg} \quad (15)$$

$$n_{H_{2(g)}-pg} = 0.09 \cdot n_{pg} \quad (16)$$

By substituting Equations 14 to 16 into Equation 13, the expression for $n_{O_{2(g)}-ST}$ becomes:

$$n_{O_{2(g)}-ST} = \left(0.07 \cdot n_{pg} \cdot 2 + \frac{0.14 \cdot n_{pg}}{2} + \frac{0.09 \cdot n_{pg}}{2} \right) \quad (17)$$

And after simplifying, $n_{O_{2(g)}-ST}$ is equivalent to:

$$n_{O_{2(g)}-ST} = 0.255 \cdot n_{pg} \quad (18)$$

The air introduced into the limekiln is atmospheric, and it was considered to have a molar composition of 21% $O_{2(g)}$ and 79% $N_{2(g)}$. Therefore, taking this composition into account, the number of mols of stoichiometric air (n_{a-ST}) was evaluated as follows:

$$n_{a-ST} = \frac{0.255 \cdot n_{pg}}{0.21} \quad (19)$$

However, to ensure the complete burning of a fuel, it is common to use an air excess. Typical values of excess combustion air employed in limekilns, similar to the one investigated herein, are 5 to 25% [28], 10% [7], and 15 and 32% [16]. The visited company was unable to provide us with the data regarding the quantity of air fed into the limekiln. Thus, based on the characteristics of the limekiln of the industry visited and the literature data aforementioned for analogous limekilns, in this work the excess combustion air was estimated to be 15% of the stoichiometric air. So, the number of moles of air (n_a) fed into the limekiln, considering the 15% excess air, was evaluated as follows:

$$n_a = 1.15 \cdot n_{a-ST} \quad (20)$$

Substituting Equation 19 into Equation 20 and simplifying, n_a becomes:

$$n_a = 1.15 \cdot \frac{0.255 \cdot n_{pg}}{0.21} = 1.397 \cdot n_{pg} \quad (21)$$

Using the relation $n = m/MM$, in Equation 21, it results in:

$$\frac{m_a}{MM_a} = 1.397 \cdot \frac{m_{pg}}{MM_{pg}} \quad (22)$$

where the molar mass of atmospheric air (MM_a) of 28.85 kg/kmol and the molar mass of the producer gas of 28.03 kg/kmol given in Table 1 were employed. Therefore, inputting these MM values in Equation 22, it becomes:

$$m_a = 1.438 \cdot m_{pg} \quad (23)$$

Energy Balance

Figure 2(b) shows the limekiln's CV with the energy flows i (En_i) involved. In this CV, considering steady state, the sum of input energies i (En_{in-CV}) is equivalent to the sum of output energies i (En_{out-CV}) plus the energy required for calcination (En_{cr}), in order to satisfy the energy conservation principle, as expressed in Equation 24:

$$\sum En_{in-CV} = \sum En_{out-CV} + En_{cr} \quad (24)$$

and substituting in Equation 24 the energy flows (En_i), it results in:

$$En_{ls} + En_{pg} + En_a = En_{lm} + En_{eg} + En_{ls-ub} + E_{sw} + E_{wl} + En_{cr} \quad (25)$$

in which the energy flows in kW correspond to: limestone (En_{ls}), producer gas (En_{pg}), combustion air (En_a), quicklime (En_{lm}), exhaust gases (En_{eg}), calcination (En_{cr}), unburnt limestone (En_{ls-ub}), solid waste (En_{sw}) and wall loss (En_{wl}).

The energy flow of exhaust gases (En_{eg}) is characterized by the sum of the energy flows of combustion products (En_{pc}) and $CO_{2(g)}$ generated in calcination ($En_{CO_{2(g)}-cr}$), as follows:

$$En_{eg} = En_{pc} + En_{CO_{2(g)}-cr} \quad (26)$$

To determine the energy flows i (En_i) corresponding to En_{ls} , En_a , En_{lm} , En_{ls-ub} , $En_{CO_{2(g)}-cr}$, En_{pc} and En_{sw} , the Equation 27 was used, considering the constituent chemical species j

in each flow. The specific heats (Cp_j) for the species and mass flow temperatures (T_i) were presented in Table 1. The reference state temperature (T_0) considered was 298 K. The species molar flows (n_j) was determined through the molar mass conversion mentioned previously.

$$En_i = \sum_{j=1}^p \left(\int_{T_0}^{T_i} Cp_j \cdot dT \right) \cdot n_j \quad (27)$$

The calcination reaction energy (En_{cr}) is equivalent to the heats of reaction of $\text{CaCO}_{3(s)}$ ($\Delta h_{R-\text{CaCO}_{3(s)}}^\circ$) and $\text{CaCO}_3 \cdot \text{MgCO}_{3(s)}$ ($\Delta h_{R-\text{CaCO}_3 \cdot \text{MgCO}_{3(s)}}^\circ$), defined respectively in Equations 1 and 2, multiplied by the molar flows of these chemical species present in the limestone, as follows:

$$En_{cr} = \left(\Delta h_{R-\text{CaCO}_{3(s)}}^\circ \cdot n_{\text{CaCO}_{3(s)}} \right) + \left(\Delta h_{R-\text{CaCO}_3 \cdot \text{MgCO}_{3(s)}}^\circ \cdot n_{\text{CaCO}_3 \cdot \text{MgCO}_{3(s)}} \right) \quad (28)$$

Values of thermal energy flow lost through the limekiln walls (En_{wl}) are mentioned in the literature as being 4.6 and 9.1% [16], and 9.67 and 14.69% [6] of the available energy. Hence, because of the characteristics of the limekiln investigated herein, En_{wl} was considered to be 20% of the energy provided by the producer gas (En_{pg}), thus:

$$En_{wl} = 0.2 \cdot En_{pg} \quad (29)$$

Similar ways to estimate En_{wl} was also performed by [7].

The energy flow of producer gas (En_{pg}) was calculated through the sum of heats of combustion of the species j (Δh_{R-j}°) that undergo combustion plus their integrals of Cp_j as a temperature function, and each multiplied by the respective molar flows (n_j), as follows:

$$\begin{aligned} En_{pg} = & \left(\Delta h_{R-\text{CH}_4(g)}^\circ + \int_{660.30}^{298.15} Cp_{\text{CH}_4(g)} \cdot dT \right) \cdot n_{\text{CH}_4(g)} + \left(\Delta h_{R-\text{CO}(g)}^\circ + \int_{660.30}^{298.15} Cp_{\text{CO}(g)} \cdot dT \right) \cdot \\ & n_{\text{CO}(g)} + \left(\Delta h_{R-\text{H}_2(g)}^\circ + \int_{660.30}^{298.15} Cp_{\text{H}_2(g)} \cdot dT \right) \cdot n_{\text{H}_2(g)} + \left(\int_{660.30}^{298.15} Cp_{\text{CO}_2(g)} \cdot dT \right) \cdot n_{\text{CO}_2(g)} + \\ & \left(\int_{660.30}^{298.15} Cp_{\text{N}_2(g)} \cdot dT \right) \cdot n_{\text{N}_2(g)} \end{aligned} \quad (30)$$

In Equation 30, values for $\Delta h_{R-\text{CH}_4(g)}^\circ$, $\Delta h_{R-\text{CO}(g)}^\circ$ and $\Delta h_{R-\text{H}_2(g)}^\circ$ were given in Equations 3, 4 and 5, respectively; the species Cp_j polynomials for integral calculation were provided in Table 1; the molar flows of producer gas species (n_j) can be converted to species mass flows (m_j) utilizing MM_j

values, and then m_j can be put as a function of mass flow of producer gas (m_{pg}) employing its chemical composition supplied in Table 1. So, doing this procedure and then simplifying, Equation 30 can be transformed into an equation of En_{pg} as a function of m_{pg} , as follows:

$$En_{pg} = 1.2869 \cdot m_{pg} \quad (31)$$

The energy flow of combustion products (En_{pc}) was determined through Equation 27 principle, for its constituent j species, in this way:

$$En_{pc} = \left(\int_{298.0}^{471.4} Cp_{H_2O(g)} \cdot dT \right) \cdot n_{H_2O(g)} + \left(\int_{298.0}^{471.4} Cp_{CO_2(g)} \cdot dT \right) \cdot n_{CO_2(g)} + \left(\int_{298.0}^{471.4} Cp_{O_2(g)} \cdot dT \right) \cdot n_{O_2(g)} + \left(\int_{298.0}^{471.4} Cp_{N_2(g)} \cdot dT \right) \cdot n_{N_2(g)} \quad (32)$$

In Equation 32, Cp_j polynomials were also given in Table 1; through stoichiometry of the combustion reactions described in Equations 3, 4 and 5 the species molar flows of combustion products can be represented as function of molar flows of producer gas reacting species and combustion air; and then these reacting species molar flows of producer gas and combustion air can be converted to mass flows m_{pg} and m_a employing the chemical compositions given in Table 1, air molar proportion considered and MM values. Therefore, doing this procedure in Equation 32 and then simplifying, En_{pc} can be put in terms of m_{pg} and m_a , as follows:

$$En_{pc} = 0.06822 \cdot m_{pg} + 0.04014 \cdot m_a \quad (33)$$

Equation system

An equation system can be defined by the set of eight Equations 10, 11, 23, 25, 26, 29, 31 and 33, having the following eight variables as output data: m_{pg} , m_a , m_{pc} , m_{eg} , En_{pg} , En_{eg} , En_{pc} e En_{wl} , and the remaining variables as input data previously calculated. To solve this equation system, the Solver add-in was employed in Excel software with GRG Nonlinear solution method, multiple starting points, and convergence of $1 \cdot 10^{-10}$. Overall solutions were found.

With all mass and energy flows determined, it was then possible to calculate the exergy balance variables described in the following section.

Exergy Balance

The limekiln's CV is presented in Figure 2(c) with representation of the exergy flows i (Ex_i) involved. Through an exergy balance, and considering steady state, the sum of input exergy flows i (Ex_{in-CV}) is equivalent to the sum of output exergy flows i (Ex_{out-CV}), plus the destroyed exergy flow (Ex_D), thus [16, 29]:

$$\sum Ex_{in-CV} = \sum Ex_{out-CV} + Ex_D \quad (34)$$

therefore, replacing the exergy flows, it results in:

$$Ex_{ls} + Ex_{pg} + Ex_a = Ex_{lm} + Ex_{eg} + Ex_{ls-ub} + Ex_{sw} + Ex_{wl} + Ex_D \quad (35)$$

where the exergy flows in kW correspond to: limestone (Ex_{ls}), producer gas (Ex_{pg}), combustion air (Ex_a), quicklime (Ex_{lm}), exhaust gases (Ex_{eg}), unburnt limestone (Ex_{ls-ub}), solid waste (Ex_{sw}), wall loss (Ex_{wl}) and destroyed exergy (Ex_D).

In Equation 35, each exergy flow i (Ex_i) for solid and gas flows corresponds to the sum of their fractions of physical ($Ex_{ph;i}$) and chemical ($Ex_{ch;i}$) exergies i , thus:

$$Ex_i = Ex_{ph;i} + Ex_{ch;i} \quad (36)$$

The physical exergy ($Ex_{ph;i}$) for a flow i of solids or gases was calculated through the sum of physical exergies of constituent chemical species j of that flow, as follows [29]:

$$Ex_{ph;i} = \sum_{j=1}^p [(h_j - h_0) - T_0 \cdot (s_j - s_0)] \cdot n_j \quad (37)$$

in which h_j and s_j are the specific enthalpy and entropy of the chemical species j evaluated at the flow conditions, h_0 and s_0 are the specific enthalpy and entropy of the chemical species j at dead state, n_j is the molar flow of the chemical species j , and T_0 is the temperature at dead state, which was considered 298 K and 101.325 kPa. In Equation 37, enthalpy and entropy variations were calculated with Equations 38 and 39, respectively, considering specific heat varying with temperature [29]:

$$(h_j - h_0) = \int_{T_0}^{T_i} Cp_j dT \quad (38)$$

$$(s_j - s_0) = \int_{T_0}^{T_i} \frac{C_{p_j}}{T} dT - R \cdot \ln \frac{P_i}{P_0} \quad (39)$$

In Equation 39, the pressure term is assessed solely for gases, and not for liquids and solids. Nevertheless, the system is open and is at reference state pressure (P_0), and the pressure of the flows i (P_i) are equal to P_0 . So, the pressure term is negligible for gases since $P_i = P_0$ [29].

The chemical exergies ($Ex_{ch;i}$) for solid flows i were determined as follows [30]:

$$Ex_{ch;i} = \sum_{j=1}^p ex_{ch;j} \cdot n_j \quad (40)$$

where the specific chemical exergies ($ex_{ch;j}$) of substances j are tabulated [31].

To determine chemical exergies ($Ex_{ch;i}$) of flows i composed of mixture of gases j , the following equation was employed [30]:

$$Ex_{ch;i} = \left(\sum_{j=1}^p x_j ex_{ch;j} + R \cdot T_0 \cdot \sum_{j=1}^p x_j \cdot \ln x_j \right) \cdot n_i \quad (41)$$

in which x_j , R and n_i are, respectively, mole fraction of chemical species j in the mixture, universal gas constant and molar flow of the gas mixture i .

The wall heat loss exergy flow (Ex_{wl}) can be estimated to be 0.09 kW/(kg_{quicklime}/h) [16].

Energy and exergy efficiencies and specific energy consumption

In calcination companies, the energy efficiency of a limekiln (η_{en}) is conventionally determined by dividing the energy necessary for calcination (En_{cr}) by the product of fuel consumption and the lower calorific value of the fuel [32]. Therefore, considering the producer gas, the energy efficiency of the limekiln was calculated as follows:

$$\eta_{en} = \frac{En_{cr}}{V_{pg} \cdot LHV_{pg}} \quad (42)$$

where V_{pg} and LHV_{pg} are the volumetric consumption and lower calorific value of the producer gas, respectively.

On the other hand, when considering the gasification of eucalyptus wood into producer gas, the overall energy efficiency ($\eta_{en-overall}$) of the calcination process was assessed based on the energy provided by the eucalyptus wood:

$$\eta_{en-overall} = \frac{En_{cr}}{m_{ew} \cdot LHV_{ew}} \quad (43)$$

in which m_{ew} and LHV_{ew} are the mass flow and lower calorific value of the eucalyptus wood, respectively.

The exergy efficiency of the limekiln (η_{ex}) was determined as follows [16]:

$$\eta_{ex} = \frac{Ex_{ch;lm}}{Ex_{pg}} \quad (44)$$

where $Ex_{ch,lm}$ is the chemical exergy of the quicklime and Ex_{pg} is the exergy of producer gas consumed by the limekiln.

Similar to the approach employed for the overall energy efficiency, the overall exergy efficiency ($\eta_{ex-overall}$) of the calcination process was calculated as follows:

$$\eta_{ex-overall} = \frac{Ex_{ch;lm}}{Ex_{ew}} \quad (45)$$

in which Ex_{ew} is the exergy flow of eucalyptus wood consumed in the calcination process. The physical exergy part of the eucalyptus wood ($Ex_{ph;ew}$) is negligible as it is at dead state temperature, and the fraction of chemical exergy of the eucalyptus wood ($Ex_{ch;ew}$) was determined based on its chemical composition, specifically for dry biomass, in kW [33]:

$$Ex_{ch;ew} = (1812.5 + 295.606 \cdot C + 587.354 \cdot H + 17.506 \cdot O + 17.735 \cdot N - 31.8 \cdot A) \cdot m_{ew} \quad (46)$$

where C , H , O , N , and A are the percentages of carbon, hydrogen, oxygen, nitrogen, and ash, respectively, that constitute the eucalyptus wood.

The specific energy consumption of the limekiln (SEN), which characterizes the amount of fuel energy consumed per ton of produced quicklime (m_{lm}), was determined as follows [6]:

$$SEN = \frac{V_{pg} \cdot LHV_{pg}}{m_{lm}} \quad (47)$$

And the overall specific energy consumption ($SEN_{overall}$) of the calcination process was assessed, taking into account the energy consumption from eucalyptus wood, in this way:

$$SEN_{overall} = \frac{m_{ew} \cdot LHV_{ew}}{m_{lm}} \quad (48)$$

ANALYSES AND DISCUSSIONS OF RESULTS

In this chapter, the outcomes of mass, energy, and exergy balances obtained for the investigated limekiln's CV, referred to as "Kiln 1", which operates with producer gas as a renewable biofuel derived from eucalyptus wood gasification, are presented and discussed.

These results obtained for Kiln 1 were primarily compared with findings from two similar vertical annular shaft limekilns that operate using non-renewable fossil fuels. These two limekilns, designated as Kiln 2 and Kiln 3, were investigated by [16] and [34], respectively, and utilize oil and lignite dust as non-renewable fossil fuels. Moreover, other literature data for analogous vertical annular shaft limekilns were also compared with the Kiln 1 investigated herein, in which case the citations were provided accurately.

Literature data were presented as provided by the references, and with temperatures standardized in degrees Celsius. The operational data of limekilns of the same type vary even among literature data. This occurs due to, for example, differences in local temperature, control systems, chemical compositions of limestone, quicklime and of the fuel, and substance flow rates. Thus, the comparisons made in this work were generally made in specific terms and are similar to those made in the literature [6, 16], and were not intended to affirm that one fuel is better than another in terms of energy or exergy. The comparisons were made in this work to verify that the methodology used is feasible and capable of providing operational data from a company using locally available sustainable biofuel as a substitute for traditional fossil fuels.

Mass Balance Results

Table 2 shows the results of mass flows and by percentage of constituent chemical species for Kiln 1. It can be seen that the sum of input mass flows in Kiln 1 (m_{in-CV}) is equivalent to the sum of output mass flows (m_{out-CV}), according to the mass conservation principle presented in Equation 9.

From Table 2, it is noted that Kiln 1 operates with a proportion of 0.767 kg of CO₂ from calcination per kg of quicklime produced. This same parameter is commonly reported in the literature for the characterization of calcination processes, with typical values of 0.751 [35], 0.786 [6] and

0.783–0.786 [36] kg of CO₂ per kg of quicklime produced. These data are in accordance with the result achieved for Kiln 1.

Considering the total amount of CO₂ emitted, including the calcination and fuel combustion, Kiln 1 works with an emission ratio of 1.427 kg of CO₂ per kg of quicklime produced. This parameter is also traditionally reported in the literature as a specification of calcination processes. And this result for total quantity of CO₂ emitted per kg of quicklime produced attained in Kiln 1, are also in consonance with literature results with values of 1.092 [35], 1.113 – 1.129 [36], 1.221 – 1.401 [6] kg of CO₂ per kg of quicklime produced. These emission ratios were not reported for Kilns 2 and 3 by the literature.

As previously mentioned, note that limekiln specifications can vary from one literature source to another. This occurs, for example, due to differences in local temperatures, control systems, limekiln design, chemical compositions of the limestone, quicklime and of the fuel, and substances flow rates.

Table 2

Energy Balance Results

In Table 3, the results of energy flows and in terms of chemical species percentage for the Kiln 1 were presented. As indicated in Equation 24, it is noted that the sum of energy flows entering CV (En_{in-CV}) is equivalent to the sum of energy flows leaving CV (En_{out-CV}) plus the energy required for calcination (En_{cr}), thus satisfying the energy conservation principle.

Note that of the total input energy flow provided by the producer gas, this is mostly distributed to the limestone calcination (En_{cr}). This was expected, because limestone calcination is an industrial process that requires a large amount of energy [16].

The exhaust gases, which include En_{pc} and $En_{CO_2(g)-cr}$, have a considerable energy content released into the atmosphere, and are therefore wasted. Hence, the heat from the exhaust gases of Kiln 1 could be recovered. This could be achieved with the implementation of a recirculation system directing the gases into the limekiln. Doing so would preheat the limestone entering the equipment at ambient temperature, contributing to its calcination. Consequently, this could reduce the consumption of producer gas. This gas recirculation technology is commonly used in the lime sector [15], however the visited company lacks this equipment.

Table 3

In Figure 3, a Sankey diagram comparison of energy flows results for Kilns 1, 2 and 3 was made. It is perceived that the limestone and combustion air energy input flows in Kiln 1 were considered insignificant, as both flows are at ambient temperature. Similarly, in Kilns 2 and 3 the limestone and combustion air input energies represent insignificant fractions, with a maximum of 1.1% for combustion air energy in Kiln 3.

The fuel energy flow corresponds to the majority fraction of the sum of energies entering the three limekilns. In Kiln 1, the producer gas energy corresponds to 100%, being, therefore, in accordance with the fossil fuels percentages, oil and lignite dust, used in Kilns 2 and 3, respectively, 98.2 and 98.4%.

Regarding the output flows, the energy of exhaust gases is 12.4% of the sum of input energies in Kiln 1, while for Kilns 2 and 3 it is equivalent to 29.3 and 23.2%, respectively. It can be noted that the higher the output temperature of the exhaust gases, the greater the energy wasted in this flow. This is evidenced because the Kiln 2 operates with the highest output temperature (455.0 °C) and fraction of exhaust gases energy (29.3%), while the Kiln 1 investigated herein works with the lowest values of these parameters, 198.2 °C and 12.4%, respectively.

In Kiln 1, the quicklime energy corresponds to 0.6%, being similar to 0.6% in Kiln 3, while in Kiln 2 it represents 4.8%. It is observed that in Kiln 2, the quicklime leaves the equipment at a considerably higher temperature (277.0 °C) compared to Kilns 1 (60.0 °C) and 3 (35.0 °C), which results in a significant waste of 4.8% of the energy supplied.

The wall loss energy corresponds to 20.0% in Kiln 1, being higher than in Kiln 2 (9.1%) and Kiln 3 (4.6%). In Kiln 1, the solid waste and unburnt limestone energies have the lowest energy fractions, being 0.002 and 0.03%, respectively. These two results are also consistent with Kilns 2 and 3, as they were disregarded.

As in Kiln 1, in Kilns 2 and 3 the energy content of the exhaust gases could be recovered through the gas recirculation system mentioned in this section. The heat recovered from the exhaust gases can contribute to limestone calcination and reduce fuel consumption and manufacturing cost. In this way, according to Equation 42 the energy efficiency (η_{en}) can be increased. Another option to further improve the energy efficiency of the limekilns would be to apply an operational control method in order to find optimal operational values of variables such as the exhaust gas and quicklime output temperatures. This type of operational control method was also employed by [32] for operational variables of a vertical industrial limekiln, achieving reductions in fuel and raw material consumption and environmental impacts, in addition to improving the quality of the quicklime.

In the Sankey diagrams shown in Figure 3, it can be seen that the energy required for calcination corresponds to the largest portion of the total input energy, being 66.9% in Kiln 1, similar to Kiln 3 with 71.6%, while in Kiln 2 it was 56.8%. The suitability of the methodology applied in this work can be perceived through the consistency of the results achieved for the Kiln 1 investigated herein with those of Kilns 2 and 3 in the literature.

Figure 3

Exergy Balance Results

Table 4 shows the results achieved for exergy flows of the CV of Kiln 1, and the contributions of physical and chemical exergies in each flow. The temperatures and percentages of the exergy of each flow were also presented in relation to the total exergy entering the equipment. It can be seen that the Equation 34 is being satisfied, because the sum of exergy flows entering CV (Ex_{in-CV}) corresponds to the sum of exergy flows leaving it (Ex_{out-CV}) plus the destroyed exergy flow (Ex_D).

Table 4

Figure 4 shows a Sankey Diagram comparison of the results of exergy flows obtained in Kilns 1, 2 and 3. The temperature, percentages of physical and chemical exergies in each flow were also presented. The Equation 34 is being satisfied in all limekilns, where the exergies that enter these, are equivalent to the exergies that leave plus the destroyed exergy.

Analyzing Table 4 and Figure 4, it is noted that the highest physical exergy content, which is recoverable, is related to the exhaust gas output flow in the three limekilns. The amount of physical exergy of quicklime is low compared to its chemical exergy in the three kilns. This reinforces the importance of implementing a gas recirculation system and application of the operational control method for optimal values of variables, such as the exhaust gas output temperature. The recovery of physical exergy from exhaust gases and quicklime can support limestone calcination and reduce fuel consumption, and according to Equation 44, increase the exergy efficiency (η_{ex}) of limekilns.

As shown in Figure 4, the limestone exergy flow has no physical exergy fraction in all kilns, as this flow is at dead state temperature. Therefore, the limestone chemical exergy portion corresponds to its total exergy, being 0.6, 5.6 and 6.1% of the sum of input exergies, in Kilns 1, 2 and 3, respectively.

The combustion air exergy represents the smallest contribution of the sum of input exergies in all limekilns. In Kiln 1, the physical and chemical exergies of combustion air were disregarded because the air is atmospheric under dead state conditions. Similarly, the combustion air physical exergy is negligible in Kiln 3 and zero in Kiln 2. In Kilns 2 and 3, combustion air exergies have contributions of 1.7 and 3.3%, respectively.

The fuel exergy flow corresponds to the largest contribution of the sum of input exergies in all limekilns. In Kiln 1, the producer gas exergy, the renewable biofuel, has a contribution of 99.4%, comprised mostly by 96.5% of chemical exergy. Similarly, the fossil fuel exergies in Kilns 2 and 3 are equivalent to 92.7 and 90.6%, respectively, being composed solely of chemical exergy.

As seen in Figure 4, for output flows, the quicklime exergy is mainly comprised of chemical exergy, and has contributions of 42.0, 38.1 and 41.0% in Kilns 1, 2 and 3, respectively, in relation to total input exergy.

The exhaust gases exergies correspond to similar percentages of 14.6, 14.3 and 11.2% in Kilns 1, 2 and 3 respectively. In Kilns 2 and 3, the exhaust gases exergies have contributions of 45.6 and 45.9% of chemical exergy, respectively, and 54.4 and 54.1% of physical exergy, respectively. Conversely, the exhaust gases exergy in Kiln 1 has 19.1% contribution of physical exergy and 80.9% of chemical exergy. Kiln 1 operates with exhaust gases at considerably lower temperature (198.2 °C) compared to Kiln 2 (455.0 °C) and 3 (315.0 °C), so it is understandable that Kiln 1 has lower contribution of physical exergy.

The wall loss exergies have similar percentages of 7.1, 6.1 and 1.3% in Kilns 1, 2 and 3, respectively. The unburnt limestone and solid waste exergies in Kiln 1 have insignificant contributions of 0.02 and 0.01%, respectively, and in Kilns 2 and 3 they were disregarded.

Through the exergy balance expressed in Equation 34, the sum of output exergies from Kilns 1, 2 and 3 has similar percentages of respectively 63.7, 58.5 and 53.5% of the sum of input exergies. Consequently, the destroyed exergy corresponds to the remaining fraction of total input exergy, being 36.3, 41.5 and 46.5% in Kilns 1, 2 and 3, respectively. The destroyed exergy is inherent to the characteristic irreversibilities of real thermodynamic processes according to the second law of thermodynamics. Examples of sources of irreversibilities in limekilns are the chemical reactions of combustion and calcination, and heat transfer processes in the equipment [16]. As can be seen, the destroyed exergy in the Kiln 1 investigated herein was 5.2 and 10.2% lower than in Kilns 2 and 3 of the literature, respectively.

In Figure 4, it is perceived that the total input exergy in Kiln 1 is distributed in the following descending order: quicklime exergy (42.0%), destroyed exergy (36.3%), exhaust gases (14.6%), wall loss (7.1%), unburnt limestone (0.02%) and solid waste (0.01%). Similarly, it can be seen that in Kilns

2 and 3 the total input exergy was mostly distributed in destroyed exergy, which is followed by quicklime, exhaust gases, and wall loss exergies, these three in the same decreasing order obtained in Kiln 1. The correspondence of the results attained for Kiln 1 with Kilns 2 and 3 in the literature, indicates the suitability of the applied analysis methodology for scrutinizing the limekilns.

Figure 4

Efficiencies and *SEN* results

This section presents the results achieved in the present work and also some found in the literature for similar vertical limekilns. The specific energy (*SEN*) found in the present study for the Kiln 1 was 4.8 GJ of producer gas energy consumed per ton of quicklime produced, in agreement with the literature *SEN* values of 4.0 – 4.8 [15], 4.4 [34], 4.7 [16], and 5.45 – 5.82 GJ/t [6]. The *SEN* value of Kiln 1 is in agreement with those of Kilns 2 (4.7 GJ/t) and 3 (4.4 GJ/t), studied by [16] and [34] respectively.

And considering the overall calcination process, the overall specific energy ($SEN_{overall}$) achieved was 7.6 GJ of eucalyptus wood energy consumed per ton of quicklime produced, which is higher than the literature *SEN* values aforementioned. According to Equations 47 and 48, lower *SEN* values are desirable, as less fuel energy is consumed to produce quicklime.

Considering the producer gas energy consumption, the energy efficiency (η_{en}) evaluated with Equation 42 for the Kiln 1 was 54.6%, which is in compliance with the η_{en} found for similar limekilns operating with fossil fuels studied in the literature, with values of: 54.68 – 58.33 [6], 57.8 (Kiln 2) [16], 72.8 (Kiln 3) [34] and 65 – 77% [15].

Considering the eucalyptus wood energy consumption, the overall energy efficiency ($\eta_{en-overall}$) assessed with Equation 43 was 42.0%, which is lower than the η_{en} aforementioned by the literature.

When considering the exergy consumption of producer gas, the exergy efficiency (η_{ex}) determined using Equation 44 for Kiln 1 was 42.2%. This value aligns with η_{ex} values reported in the literature for similar limekilns performing with fossil fuels, such as 40.0 [7], 40.0 (Kiln 2) [16] and 45.3% (Kiln 3) [34].

And considering the eucalyptus wood exergy consumption, the overall exergy efficiency ($\eta_{ex-overall}$), calculated using Equation 45, was 23.6%, being lower than the η_{ex} mentioned in the literature cited previously.

The efficiency of Kiln 1 using producer gas as a biofuel does not present an advantage compared to the efficiency of limekilns employing traditional fossil fuels. However, the authors emphasize that it was possible to propose a diagnostic of a calcination process of a company where an environmentally friendly biofuel is used with efficiencies close to those of limekilns employing conventional fossil fuels. Additionally, the company reported that the use of the sustainable biofuel in its calcination process is due to its low cost compared to fossil fuels, environmental friendliness, and compliance with atmospheric emission limits without impacting the quality of quicklime. The company could not provide us with information regarding the cost of the renewable biofuel used.

In summary, as detailed previously, to enhance the values of SEN , energy efficiency, and exergy efficiency of Kiln 1, which operates with producer gas derived from eucalyptus wood gasification, as well as of other limekilns using fossil fuels, it is essential to emphasize the significance of recovering energy and exergy from exhaust gases and heat wall loss of the equipment. This can be achieved through the implementation of a gas recirculation system, a technique already employed in the quicklime industry. Furthermore, by employing operational control methods for limekiln variables, parameters such as exhaust gas and quicklime output temperatures can be adjusted to optimal values, further enhancing energy and exergy efficiencies, as well as SEN of the limekilns. Additionally, the kinetic energy of the exhaust gases could be converted into electric energy through the implementation of a turbine-generator system. Thus, this electric energy could be utilized to power the electric equipment of the calcination process, including panels and air blowers.

CONCLUSIONS

This work conducts energy and exergy diagnostics of a vertical industrial limekiln, which uses producer gas as renewable biofuel produced from eucalyptus wood gasification. Industrial data, coupled with some literature data for equipment characterization, were utilized in these diagnostics. The obtained results were compared with those from similar limekilns using fossil fuels. The Specific Energy Consumption (SEN) for the producer gas-operated limekiln was $4.8 \text{ GJ/t}_{\text{quicklime}}$, along with energy (η_{en}) and exergy (η_{ex}) efficiencies of 54.6% and 42.2%, respectively. These results align with those found by literature for analogous limekilns utilizing fossil fuels. In overall terms, the overall energy ($\eta_{en-overall}$) and exergy ($\eta_{ex-overall}$) efficiencies were 42.0 and 23.6% respectively, being lower than literature values. The $SEN_{overall}$ ($7.6 \text{ GJ/t}_{\text{quicklime}}$) was higher than the literature results. To enhance the performance of both renewable biofuel-operated and fossil fuel-operated limekilns, potential areas for energy and exergy recovery were identified. These include mainly recovering heat from exhaust gases, reducing thermal losses through limekiln walls, and deployment of operational

control methods to adjust variables such as exhaust gas and quicklime temperatures. These findings provide valuable insights for researchers exploring the adoption of renewable biofuels like eucalyptus wood-derived producer gas as alternatives to conventional fossil fuels in limekilns.

ACKNOWLEDGMENTS

The authors acknowledge the support from CAPES (Coordenação de Aperfeiçoamento de Pessoal de Nível Superior), finance code 001, and CNPq (Conselho Nacional de Desenvolvimento Científico e Tecnológico, 312248/2022-9).

REFERENCES

- [1] L. Navone, K. Moffitt, K.A. Hansen, J. Blinco, A. Payne, R. Speight, *Waste Manage.* 102 (2020) 149–160. <https://doi.org/10.1016/j.wasman.2019.10.026>
- [2]. Y. Liu, H. Shen, J. Zhang, W. Li, J. Liu, B. Liu, S. Zhang, *Constr. Build. Mater.* 395 (2023) 132292. <https://doi.org/10.1016/j.conbuildmat.2023.132292>
- [3] C. Shi, Y. Yang, *Mater.* 16 (2023) 4026. <https://doi.org/10.3390/ma16114026>
- [4] B. Li, F. Min, N. Zhang, J. Ma, Z. Li, Z. Yao, L. Zhang, *Constr. Build. Mater.* 408 (2023) 133492. <https://doi.org/10.1016/j.conbuildmat.2023.133492>
- [5] Statista (2023), Lime production by country in 2022, <https://www.statista.com/statistics/657049/production-of-lime-worldwide/> [accessed 20 October 2023]
- [6] V. Alcántara, Y. Cadavid, M. Sánchez, C. Uribe, C. Echeverri-Urbe, J. Morales, J. Obando, A. Amell, *Appl. Therm. Eng.* 128 (2018) 393–401. <https://doi.org/10.1016/j.applthermaleng.2017.09.018>
- [7] A.S. Gutiérrez, C. Vandecasteele, *Energy* 36 (2011) 2820–2827. <https://doi.org/10.1016/j.energy.2011.02.023>
- [8] A. Wolter, W. Fuchs, *ZKG Int.* 60 (2007) 45–50. https://www.researchgate.net/publication/288154779_Specific_CO2_emissions_and_the_applications_of_lime_burning_kilns
- [9] E. Smadi, A. Chinnici, B. Dally, G.J. Nathan, *Chem. Eng. J.* 475 (2023) 146165. <https://doi.org/10.1016/j.cej.2023.146165>
- [10] W. Rong, B. Li, F. Qi, S.C.P. Cheung, *Appl. Therm. Eng.* 119 (2017) 629–638. <https://doi.org/10.1016/j.applthermaleng.2017.03.090>
- [11] S. Duan, B. Li, W. Rong, *Mater.* 15 (2022) 4024. <https://doi.org/10.3390/ma15114024>
- [12] M. Greco-Coppi, C. Hofmann, D. Walter, J. Ströhle, B. Epple, *Mitig. Adapt. Strateg. Glob. Chang.* 28 (2023) 30. <https://doi.org/10.1007/s11027-023-10064-7>
- [13] S.A. Jagnade, S.K. Nayak, J.M. Korath, N.N. Viswanathan, P.B. Abhale, *Miner. Process. Extr. Metall.* 132 (2023) 141–155 <https://doi.org/10.1080/25726641.2023.2217403>
- [14] T.S. Febriatna, P.S. Darmanto, F.B. Juangsa, *Clean Energy.* 7 (2023) 313–327. <https://doi.org/10.1093/ce/zkac072>
- [15] H. Piringer, *Energy Procedia* 120 (2017) 75–95. <https://doi.org/10.1016/j.egypro.2017.07.156>
- [16] A.S. Gutiérrez, J.B.C. Martínez, C. Vandecasteele, *Appl. Therm. Eng.* 51 (2013) 273–280. <https://doi.org/10.1016/j.applthermaleng.2012.07.013>
- [17] T.P.L. Camargos, D.L.F. Pottie, R.A.M. Ferreira, T.A.C. Maia, M.P. Porto, *Energy* 165 (2018) 630–638. <https://doi.org/10.1016/j.energy.2018.09.109>

- [18] V.F. Ramos, O.S. Pinheiro, E.F. da Costa Junior, A.O.S. da Costa, *Energy* 183 (2019) 946–957. <https://doi.org/10.1016/j.energy.2019.07.001>
- [19] T.F. Anacleto, A.E.G. O. Silva, S.R. da Silva, E.F. da Costa Junior, A.O.S. da Costa, *Braz. J. Chem. Eng.* 38 (2021) 197–214. <https://doi.org/10.1007/s43153-020-00084-0>
- [20] S.R. da Silva, G. Bonanato, E.F. da Costa Junior, B. Sarrouh, A.O.S. da Costa, *Chem. Eng. Sci.* 235 (2021) 116462. <https://doi.org/10.1016/j.ces.2021.116462>
- [21] M. Höök, X. Tang, *Energy Policy* 52 (2013) 797–809. <https://doi.org/10.1016/j.enpol.2012.10.046>
- [22] European Lime Association (EuLA), *Eula Environmental Data Spreadsheet on 2011*, Brussels, Belgium (2012)
- [23] WebQC (2023), Chemical Portal, <https://www.webqc.org/> [accessed 20 October 2023]
- [24] J.M. Smith, H.C. Van Ness, M.M. Abbott, *Introduction to Chemical Engineering Thermodynamics.*, McGraw Hill (2022). ISBN: 9781260721478
- [25] C.G. Maier, K.K. Kelley, *J. Am. Chem. Soc.* 54 (1932) 3243–3246. <https://doi.org/10.1021/ja01347a029>
- [26] National Institute of Standards and Technology (2023), *Webbook*, <https://webbook.nist.gov/> [accessed 20 October 2023]
- [27] J.A. Dean, *Lange’s Handbook of Chemistry*, McGrawHill, New York (1999). ISBN: 9780070163843
- [28] H. Shahin, S. Hassanpour, A. Saboonchi, *Energy Convers. Manage.* 114 (2016) 110–121. <https://doi.org/10.1016/j.enconman.2016.02.017>
- [29] Y.A. Cengel, M.A. Boles, *Thermodynamics: An Engineering Approach*, The McGraw-Hill Companies, New York (2019). ISBN: 9781259822674
- [30] M.J. Moran, H.N. Shapiro, D.D. Boettner, M.B. Bailey, *Fundamentals of engineering thermodynamics*, John Wiley & Sons (2018). ISBN: 9781119391388
- [31] D.R. Morris, J. Szargut, *Energy* 11 (1986) 733–755. [https://doi.org/10.1016/0360-5442\(86\)90013-7](https://doi.org/10.1016/0360-5442(86)90013-7)
- [32] P.A. Ochoa George, A.S. Gutiérrez, J.B. Cogollos Martínez, C. Vandecasteele, *J. Cleaner Prod.* 18 (2010) 1171–1176. <https://doi.org/10.1016/j.jclepro.2010.03.019>
- [33] G. Song, L. Shen, J. Xiao, *Ind. Eng. Chem. Res.* 50 (2011) 9758–9766. <https://doi.org/10.1021/ie200534n>
- [34] H. Piringer, W. Werner, *ZKG Int.* 61 (2008) 46–52. https://www.researchgate.net/publication/285806720_Conversion_of_large-diameter_single_shaft_kilns_to_lignite_dust_firing_successfully_concluded

- [35] L. Shen, T. Gao, J. Zhao, L. Wang, L. Wang, L. Liu, F. Chen, J. Xue, *Renewable Sustainable Energy Rev.* 34 (2014) 337–349. <https://doi.org/10.1016/j.rser.2014.03.025>
- [36] B. Jiang, D. Xia, B. Yu, R. Xiong, W. Ao, P. Zhang, L. Cong, *J. Cleaner Prod.* 240 (2019) 118147. <https://doi.org/10.1016/j.jclepro.2019.118147>
- [37] N. Couto, A. Rouboa, V. Silva, E. Monteiro, K. Bouziane, *Energy Procedia* 36 (2013) 596–606. <https://doi.org/10.1016/j.egypro.2013.07.068>
- [38] B.L.C. Pereira, A. de C.O. Carneiro, A.M.M.L. Carvalho, J.L. Colodette, A.C. Oliveira, M.P.F. Fontes, *BioResources* 8 (2013) 4574–4592. <https://doi.org/10.15376/biores.8.3.4574-4592>
- [39] K. Sasujit, N. Homdoun, N. Tippayawong, *Energy Eng.* 119 (2022) 2149–2167. <https://doi.org/10.32604/ee.2022.022069>
- [40] T. de P. Protásio, M.V. Scatolino, A.C.C. de Araújo, A.F.C.F. de Oliveira, I.C.R. de Figueiredo, M.R. de Assis, P.F. Trugilho, *Bioenergy Res.* 12 (2019) 626–641. <https://doi.org/10.1007/s12155-019-10004-x>

FIGURE CAPTIONS

Figure 1. Vertical limekiln.

Figure 2. (a) Mass balance; (b) Energy Balance; (c) Exergy balance.

Figure 3. Energy Sankey diagrams for the kilns.

Figure 4. Exergy Sankey diagrams for the kilns.

Table 1. Data from the calcination process for the visited company.

COLLECTED DATA							
Flows	Value (kg/h)			Temperature		Value (°C)	
Limestone (m_{ls})	4455.1			Temperature A (T_A)		387.2	
Quicklime (m_{lm})	2444.7			Temperature B (T_B)		198.2	
Unburnt limestone (m_{ls-ub})	133.7			Temperature C (T_C)		60.0	
Solid waste (m_{sw})	1.5						
CO _{2(g)} from calcination (m_{CO_2-cr})	1875.2						
Eucalyptus wood (m_{ew})	5147.2						
CHEMICAL COMPOSITION DATA							
Limestone				Quicklime			
Species	Value	Reference	Species	Value	Reference		
CaCO _{3(s)}	93.35% wt		CaO _(s)	95.10% wt			
CaCO ₃ ·MgCO _{3(s)}	4.94% wt		MgO _(s)	1.90% wt			
SiO _{2(s)}	1.55% wt	This work	SiO _{2(s)}	2.73% wt		This work	
Al ₂ O _{3(s)}	0.09% wt		Al ₂ O _{3(s)}	0.15% wt			
Fe ₂ O _{3(s)}	0.07% wt		Fe ₂ O _{3(s)}	0.12% wt			
Producer gas				Eucalyptus wood			
Species	Value	Reference	Species	Value	Reference		
N _{2(g)}	50.00% vol		C	45.19% wt			
CO _(g)	14.00% vol		O	48.89% wt			
H _{2(g)}	9.00% vol	[37]	H	5.82% wt		[38]	
CO _{2(g)}	20.00% vol		N	0.10% wt			
CH _{4(g)}	7.00% vol		Ash (A)	0.10% wt			
MM _{pg}	28.03 kg/kmol		LHV _{ew}	18.27 MJ/kg		[40]	
LHV _{pg}	2.94 MJ/m ³	[39]					
SPECIFIC HEAT POLYNOMIAL COEFFICIENTS							
Species	A	B	C	D	E	Validity (K)	Equation
CaCO _{3(s)}	12.572	0.002637	0	-312000	-	298–1200	6
CaCO ₃ ·MgCO _{3(s)}	141.5	0.1359	2175000		-	298–650	7
SiO _{2(s)}	4.871	0.005365	0	-100100	-	298–847	6
Al ₂ O _{3(s)}	102.4290	38.7498	-15.9109	2.6282	-3.0076	298–2327	6
Fe ₂ O _{3(s)}	11.812	0.009697	0	-197600	-	298–960	6
CaO _(s)	6.104	0.000443	0	-104700	-	298–2000	6
MgO _(s)	47.2600	5.6816	-0.8727	0.1043	-1.0540	298–3105	8
CH _{4(g)}	1.702	0.009081	-0.000002164	0	-	298–1500	6
CO _(g)	3.376	0.000557	0	-3100	-	298–2500	6
H _{2(g)}	3.249	0.000422	0	8300	-	298–3000	6
CO _{2(g)}	5.457	0.001045	0	-115700	-	298–2000	6
O _{2(g)}	3.639	0.000506	0	-22700	-	298–2000	6
N _{2(g)}	3.28	0.000593	0	4000	-	298–2000	6
H ₂ O _(g)	3.47	0.00145	0	12100	-	298–2000	6

Table 2. Kiln 1 mass balance results.

Input		Output	
Mass flow (kg/h)	Chemical species mass (%)	Mass flow (kg/h)	Chemical species mass (%)
$m_{ls} = 4455.1$	$m_{CaCO_3(s)} = 0.9335 \cdot m_{ls}$	$m_{pc} = 6112.5$	$m_{H_2O(g)} = 0.0607 \cdot m_{pc}$
	$m_{CaCO_3 \cdot MgCO_3(s)} = 0.0494 \cdot m_{ls}$		$m_{CO_2(g)} = 0.2641 \cdot m_{pc}$
	$m_{SiO_2(s)} = 0.0155 \cdot m_{ls}$		$m_{O_2(g)} = 0.0179 \cdot m_{pc}$
	$m_{Al_2O_2(s)} = 0.0009 \cdot m_{ls}$		$m_{N_2(g)} = 0.6573 \cdot m_{pc}$
	$m_{Fe_2O_2(s)} = 0.0007 \cdot m_{ls}$		
$m_a = 3604.8$	$m_{O_2(g)} = 0.2329 \cdot m_a$	$m_{CO_2(g)-cr} = 1875.2$	-
	$m_{N_2(g)} = 0.7671 \cdot m_a$		
$m_{pg} = 2507.6$	$m_{N_2(g)} = 0.4996 \cdot m_{pg}$	$m_{sw} = 1.5$	$m_{CaCO_3(s)} = 0.0717 \cdot m_{sw}$
	$m_{CO(g)} = 0.1399 \cdot m_{pg}$		$m_{CaCO_3 \cdot MgCO_3(s)} = 0.5645 \cdot m_{sw}$
	$m_{H_2(g)} = 0.0065 \cdot m_{pg}$		$m_{SiO_2(s)} = 0.1581 \cdot m_{sw}$
	$m_{CO_2(g)} = 0.3140 \cdot m_{pg}$		$m_{Al_2O_2(s)} = 0.1457 \cdot m_{sw}$
	$m_{CH_4(g)} = 0.0401 \cdot m_{pg}$		$m_{Fe_2O_2(s)} = 0.0599 \cdot m_{sw}$
		$m_{lm} = 2444.7$	$m_{CaO(s)} = 0.9510 \cdot m_{lm}$
			$m_{MgO(s)} = 0.0190 \cdot m_{lm}$
			$m_{SiO_2(s)} = 0.0273 \cdot m_{lm}$
			$m_{Al_2O_2(s)} = 0.0015 \cdot m_{lm}$
			$m_{Fe_2O_2(s)} = 0.0012 \cdot m_{lm}$
		$m_{ls-ub} = 133.7$	$m_{CaCO_3(s)} = 0.9335 \cdot m_{ls-ub}$
			$m_{CaCO_3 \cdot MgCO_3(s)} = 0.0494 \cdot m_{ls-ub}$
			$m_{SiO_2(s)} = 0.0155 \cdot m_{ls-ub}$
			$m_{Al_2O_2(s)} = 0.0009 \cdot m_{ls-ub}$
			$m_{Fe_2O_2(s)} = 0.0007 \cdot m_{ls-ub}$
$m_{in-CV} = 10567.5$		$m_{out-CV} = 10567.5$	

Table 3. Kiln 1 energy balance results.

Input		Output	
Energy flow (kW)	Chemical species energy (%)	Energy flow (kW)	Chemical species energy (%)
$En_{ls} = 0$	$En_{CaCO_3(s)} = 0$	$En_{pc} = 315.8$	$En_{H_2O(g)} = 0.1073 \cdot En_{pc}$
	$En_{CaCO_3 \cdot MgCO_3(s)} = 0$		$En_{CO_2(g)} = 0.2340 \cdot En_{pc}$
	$En_{SiO_2(s)} = 0$		$En_{O_2(g)} = 0.0159 \cdot En_{pc}$
	$En_{Fe_2O_2(s)} = 0$		$En_{N_2(g)} = 0.6427 \cdot En_{pc}$
	$En_{Al_2O_2(s)} = 0$		
$En_a = 0$	$En_{O_2(g)} = 0$	$En_{CO_2(g)-cr} = 85.8$	-
	$En_{N_2(g)} = 0$		
$En_{pg} = 3227.1$	$En_{N_2(g)} = 0.0415 \cdot En_{pg}$	$En_{sw} = 0.1$	$En_{CaCO_3(s)} = 0.0662 \cdot En_{sw}$
	$En_{CO(g)} = 0.3168 \cdot En_{pg}$		$En_{CaCO_3 \cdot MgCO_3(s)} = 0.6265 \cdot En_{sw}$
	$En_{H_2(g)} = 0.1752 \cdot En_{pg}$		$En_{SiO_2(s)} = 0.1332 \cdot En_{sw}$
	$En_{CO_2(g)} = 0.0249 \cdot En_{pg}$		$En_{Al_2O_2(s)} = 0.1310 \cdot En_{sw}$
	$En_{CH_4(g)} = 0.4415 \cdot En_{pg}$		$En_{Fe_2O_2(s)} = 0.0431 \cdot En_{sw}$
		$En_{lm} = 18.4$	$En_{CaO(s)} = 0.9468 \cdot En_{lm}$
			$En_{MgO(s)} = 0.0234 \cdot En_{lm}$
			$En_{SiO_2(s)} = 0.0272 \cdot En_{lm}$
			$En_{Al_2O_2(s)} = 0.0016 \cdot En_{lm}$
			$En_{Fe_2O_2(s)} = 0.0010 \cdot En_{lm}$
		$En_{ls-ub} = 1.1$	$En_{CaCO_3(s)} = 0.9209 \cdot En_{ls-ub}$
			$En_{CaCO_3 \cdot MgCO_3(s)} = 0.0639 \cdot En_{ls-ub}$
			$En_{SiO_2(s)} = 0.0138 \cdot En_{ls-ub}$
			$En_{Al_2O_2(s)} = 0.0008 \cdot En_{ls-ub}$
			$En_{Fe_2O_2(s)} = 0.0005 \cdot En_{ls-ub}$
		$En_{wl} = 645.4$	-
		$En_{cr} = 2160.5^*$	$\Delta H_{R-CaCO_3(s)}^\circ = 0.9535 \cdot En_{cr}$
			$\Delta H_{R-CaCO_3 \cdot MgCO_3(s)}^\circ = 0.0465 \cdot En_{cr}$
$En_{in-cv} = 3227.1$		$En_{out-cv} + En_{cr} = 3227.1$	

Table 4. Kiln 1 exergy balance results.

Input						Output					
Flow	T (°C)	Ex _{ph} (kW)	Ex _{ch} (kW)	Ex (kW)	% _{total}	Flow	T (°C)	Ex _{ph} (kW)	Ex _{ch} (kW)	Ex (kW)	% _{total}
<i>Ex_{ls}</i>	25.0	0	19.4	19.4	0.6	<i>Ex_{lm}</i>	60.0	1.0	1293.2	1294.2	42.0
<i>Ex_a</i>	25.0	0	0	0	0	<i>Ex_{eg}</i>	198.2	86.1	363.5	449.6	14.6
<i>Ex_{pg}</i>	387.2	107.2	2957.1	3064.3	99.4	<i>Ex_{wl}</i>	-	-	-	220.2	7.1
						<i>Ex_{sw}</i>	198.2	0.02	0.15	0.17	0.01
						<i>Ex_{ls-ub}</i>	60.0	0.1	0.6	0.7	0.02
						<i>Ex_D</i>^a				1118.9	36.3
<i>Ex_{in-CV}</i>	-	107.2	2976.6	3083.8	100.0	<i>Ex_{out-CV} + Ex_D</i>		87.2	1657.4	3083.8	100.0

^aInside CV

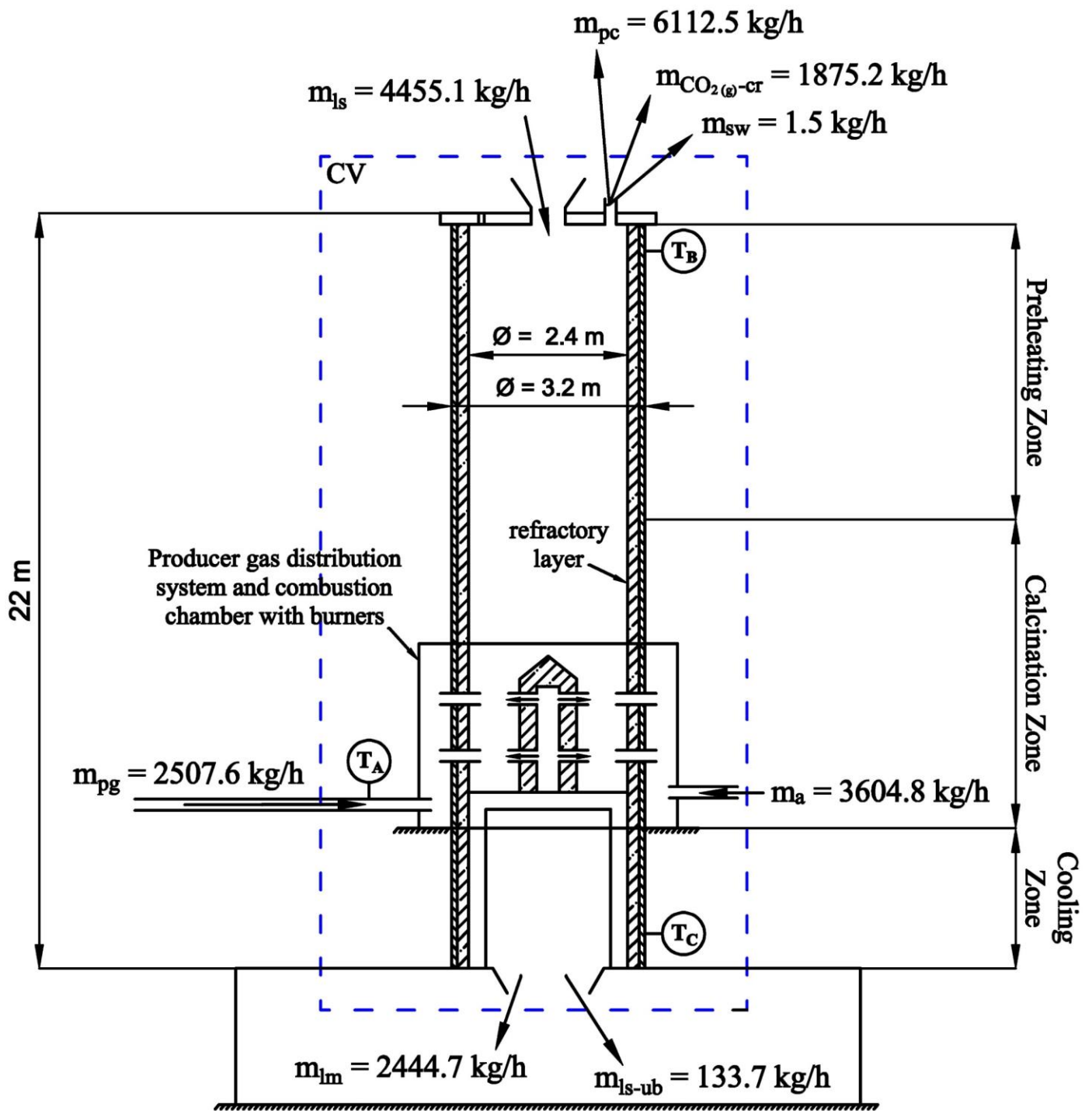
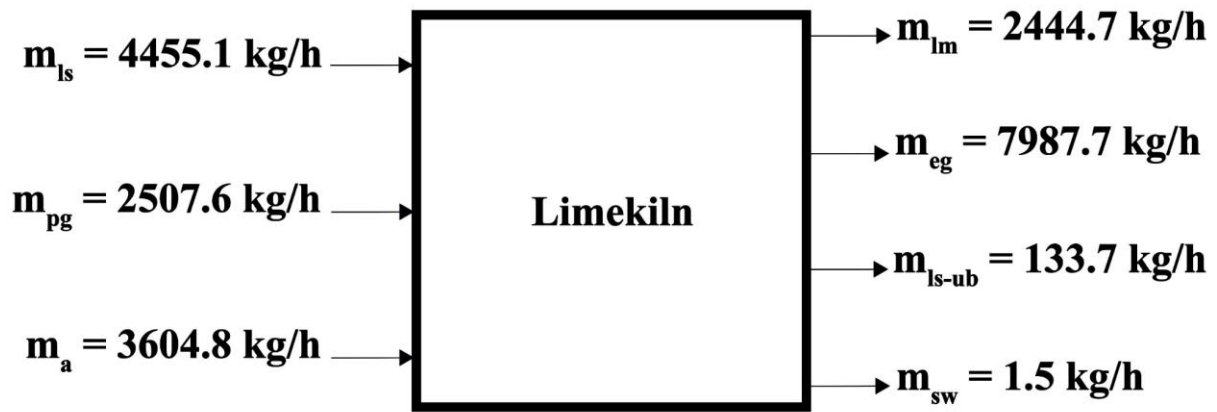
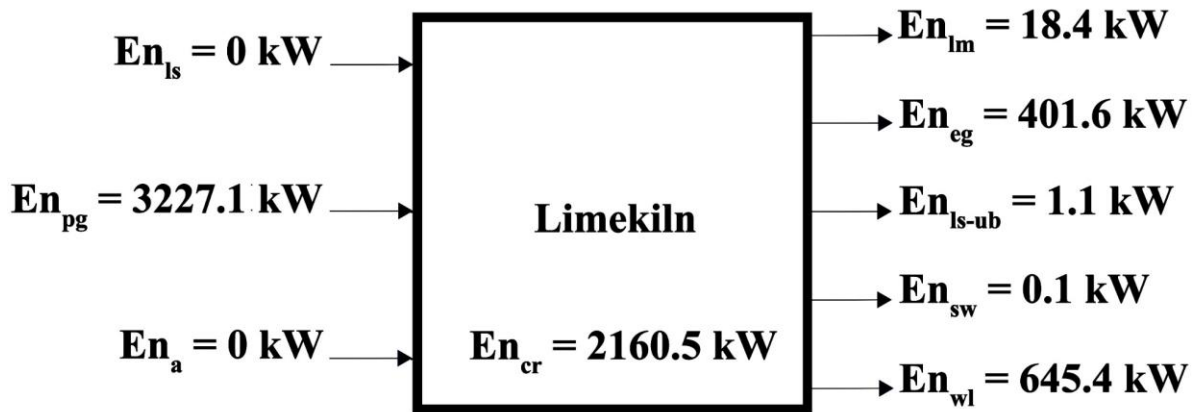


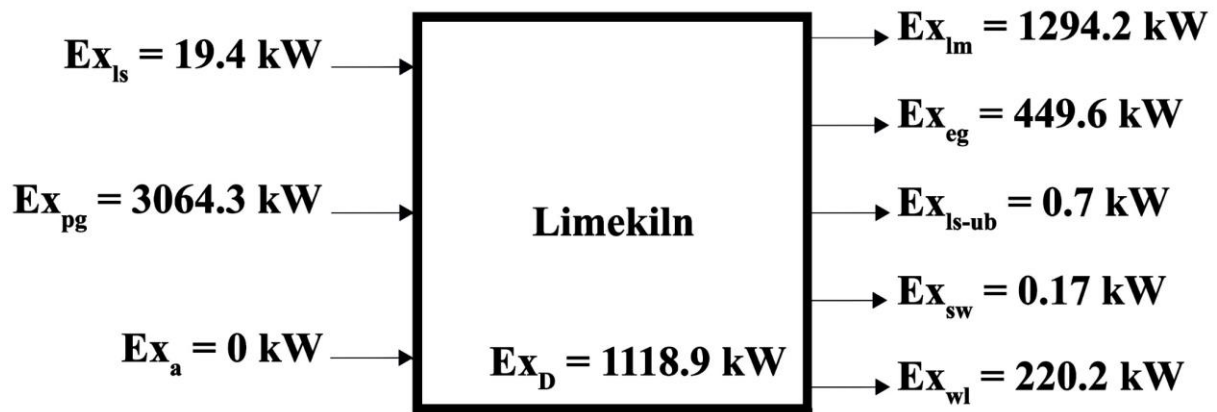
Figure 1



(a)



(b)



(c)

Figure 2

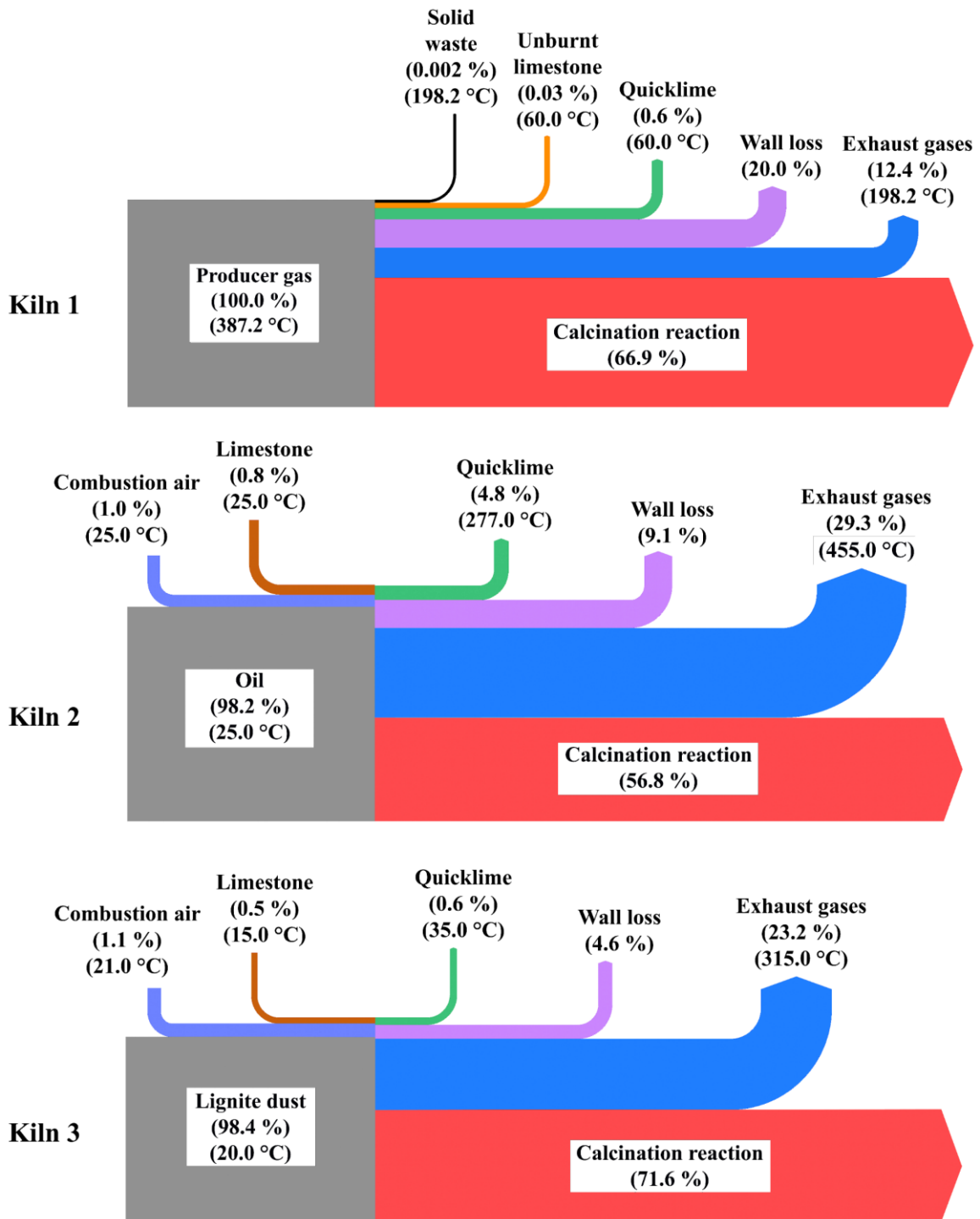


Figure 3

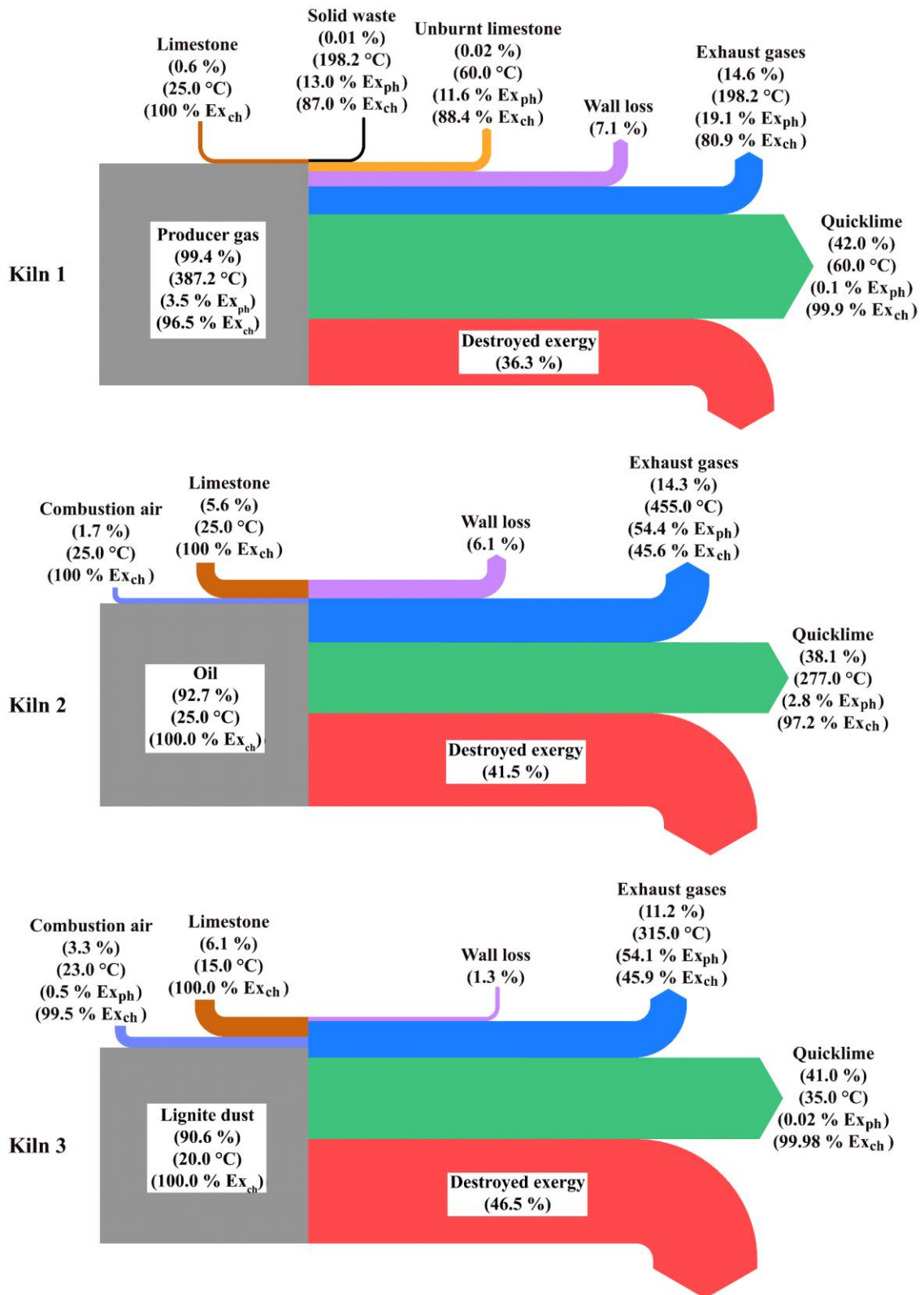


Figure 4